Int. J. Solids Structures Vol. 29, No. 24, pp. 3125–3143, 1992
Printed in Great Britain.

0020-7683/92 $5.00 + .00

AXISYMMETRIC DEFORMATION OF POROELASTIC SHELLS OF REVOLUTION

LARRY A. TABER
Department of Mechanical Engineering, University of Rochester,
Rochester, NY 14627, U.S.A.

(*Received* 30 *December* 1991)

Abstract—A linear theory is developed for axisymmetric deformation of thin poroelastic shells of revolution. With fluid–solid coupling included through Biot's consolidation theory, results are presented for cylindrical shells with an oscillating internal pressure and various surface boundary conditions on the fluid. First, the effects of fluid flow and shell inertia on the stretching behavior are studied through a separation of variables solution. Then, the bending behavior near a clamped edge is examined through an asymptotic solution of a matrix form of the governing equations. The results show that the asymptotic solution is accurate in the low frequency range, when the loading time is large compared to the consolidation time. In addition, for the examples studied, the fluid flow influences the membrane more than the bending behavior, but damping due to flow resistance is limited near resonance.

INTRODUCTION

Many biological structures, such as hearts, blood vessels and bladders, can be treated as fluid-saturated porous shells. Analyses of these and related engineering problems would be facilitated by a poroelastic shell theory, which apparently is not yet available. Laying the foundation for more general theories, this paper presents a set of linear governing equations for axisymmetric deformation of thin poroelastic shells of revolution.

Related work based on three-dimensional mixture theory has focused on nonlinear diffusion through thick-walled isotropic cylinders (Gandhi *et al.*, 1987), orthotropic cylinders (Dai *et al.*, 1991) and transversely isotropic spheres (Dai and Rajagopal, 1990). In addition, using the linear consolidation theory of Biot (1941, 1962), Kenyon (1976) studied fluid-saturated poroelastic cylinders subjected to steady and step pressure loads, and Jayaraman (1983) examined cylinders with an oscillating internal pressure. In two-dimensional formulations, Rajagopal *et al.* (1983) derived nonlinear membrane equations from the theory of mixtures, and Taber (1992) generalized the one-dimensional analysis of Biot (1964) to obtain a linear plate theory based on consolidation theory.

The present formulation extends and combines the linearized version of the nonlinear theory given by Reissner (1950) for shells of revolution and the linear theory for poroelastic plates given by Taber (1992). The shell theory is based on the following assumptions:

(1) The shell is "thin", i.e. $R/h_s \gg 1$, where R is the smallest midsurface radius of curvature and h_s is the shell thickness.
(2) Displacements are small compared to the shell thickness.
(3) Normals to the middle surface of the solid skeleton ($z = 0$) remain straight and normal during deformation. (Transverse shear deformation is ignored.)
(4) The plate is in a state of approximately plane stress, i.e. the *total* stress $\tau_z = 0$.
(5) In-plane fluid-velocity *gradients* relative to the solid are small compared to the transverse fluid-velocity gradient.

The first four assumptions are commonly employed in deriving shell theories, and the significance and validity of the last assumption are discussed by Taber (1992).

Based on this theory, results are presented for shells with oscillating internal pressures. Using a separation of variables solution, we first explore the membrane behavior of cylindrical shells with end effects ignored. Next, the governing equations are expressed in the form of a first-order vector equation, and an asymptotic solution is developed using the procedure of Steele and Skogh (1970) for shells of revolution. Results are given for a

clamped cylinder with various surface boundary conditions, and the two solutions are compared in the shell interior.

POROELASTIC SHELL THEORY

In deriving the governing equations, our procedure is similar to those of Reissner (1950) and Taber (1992). Thus, here we omit some of the specific details, with the interested reader referred to those papers.

Geometric relations

Consider a thin poroelastic shell of revolution with axis of symmetry y (Fig. 1). Let $\mathbf{u}(s, z, t)$ and $\mathbf{u}_f(s, z, t)$ represent the displacements of the solid and fluid, respectively, where s is the meridional coordinate along the middle surface, z is the distance from this surface, and t is time.

During an axisymmetric (torsionless) deformation, a middle-surface element at a radius r and meridional angle ϕ undergoes a displacement $\mathbf{u}(s, 0, t) = w\mathbf{e}_z + u\mathbf{e}_\phi = h\mathbf{e}_r + v\mathbf{e}_y$ and a meridional rotation χ. (Figure 1 shows the unit vectors $\mathbf{e}_i$.) The geometry gives the relations between the displacement components

$$h = u\cos\phi + w\sin\phi, \quad v = u\sin\phi - w\cos\phi. \tag{1}$$

Under assumptions (1)–(3), the strains in the solid skeleton are

$$e_\phi = \varepsilon_\phi + z\kappa_\phi, \quad e_\theta = \varepsilon_\theta + z\kappa_\theta, \tag{2}$$

where the middle surface strains are

$$\varepsilon_\phi = h'\cos\phi + v'\sin\phi, \quad \varepsilon_\theta = h/r \tag{3}$$

and the curvature measures are

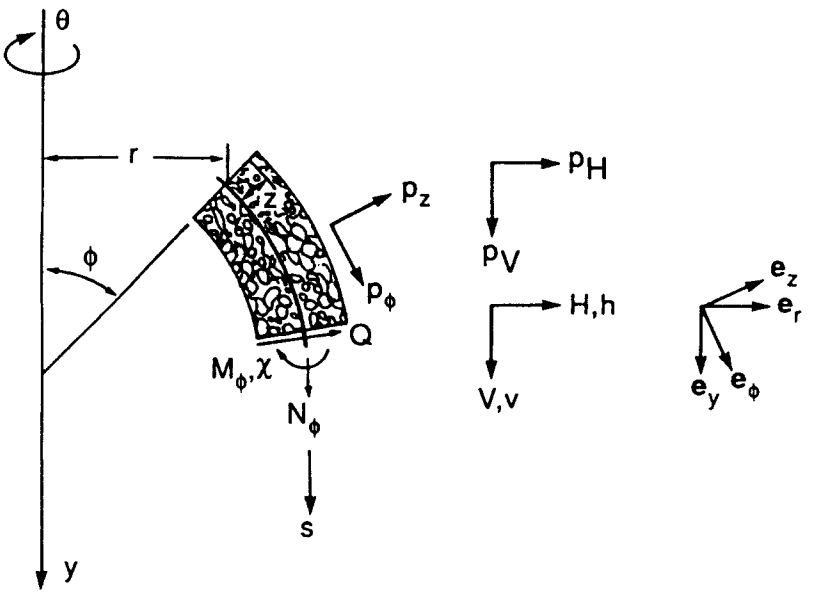

Fig. 1. Poroelastic shell geometry.

$$\kappa_\phi = \chi', \quad \kappa_\theta = \chi \cos\phi / r \tag{4}$$

with prime denoting differentiation with respect to s. In terms of displacements, the rotation is

$$\chi = u/r_1 - w', \tag{5}$$

where r_1 and r_2 are the meridional and circumferential radii of curvature, respectively, and the geometry gives

$$\mathrm{d}s = r_1 \,\mathrm{d}\phi, \quad r = r_2 \sin\phi. \tag{6}$$

Here, we also define the fluid filtration

$$\zeta = \phi_f(e - e_f) \tag{7}$$

and the solid and fluid dilatations

$$e = \nabla \cdot \mathbf{u} = e_\phi + e_\theta + e_z, \quad e_f = \nabla \cdot \mathbf{u}_f, \tag{8}$$

with ϕ_f being the porosity and e_z the transverse normal strain.

Equilibrium

In terms of the *total* stresses $\tau_i(s, z, t)$ (per unit area of bulk material), the stress and moment resultants are (Fig. 1)

$$(N_\phi, N_\theta, Q) = \int (\tau_\phi, \tau_\theta, \tau_{\phi z})\,\mathrm{d}z,$$

$$(M_\phi, M_\theta) = \int (\tau_\phi, \tau_\theta) z \,\mathrm{d}z, \tag{9}$$

where $\int \equiv \int_{-h_w/2}^{h_w/2}$. Following Reissner (1950), we express the equilibrium equations in terms of the horizontal and vertical components of the stress resultants

$$H = N_\phi \cos\phi + Q \sin\phi, \quad V = N_\phi \sin\phi - Q\cos\phi \tag{10}$$

and the (middle) surface tractions

$$p_H = p_\phi \cos\phi + p_z \sin\phi, \quad p_V = p_\phi \sin\phi - p_z \cos\phi, \tag{11}$$

where p_z and p_ϕ are the normal and tangential loads per unit bulk reference-surface area. Then, the equations of vertical force, horizontal force and moment equilibrium are

$$\begin{aligned} (rV)' &= -rp_V, \\ (rH)' &= N_\theta - rp_H, \\ (rM_\phi)' &= M_\theta \cos\phi + rQ. \end{aligned} \tag{12}$$

Constitutive relations

In terms of the total stresses and the fluid (pore) pressure p_f, the three-dimensional constitutive relations are (Biot and Willis, 1957)

$$\begin{aligned} \tau_\phi &= 2\mu e_\phi + \lambda e - \alpha p_f, \\ \tau_\theta &= 2\mu e_\theta + \lambda e - \alpha p_f, \end{aligned}$$

$$\tau_z = 2\mu e_z + \lambda e - \alpha p_f,$$
$$p_f = F(\zeta - \alpha e), \tag{13}$$

where λ and μ are the Lamé constants for the solid skeleton, α characterizes the compressibility of the material comprizing the solid skeleton relative to that of the drained skeleton, and F is a modified fluid modulus [see eqns (32) and (33)]. Biot and Willis (1957) showed that $\phi_f \leqslant \alpha \leqslant 1$ and that, for incompressible solid and fluid components, $\alpha = 1$ and $F = \infty$. Note also that the fluid–solid coupling disappears if $\alpha = 0$ (no pores) or if $p_f = 0$ (no fluid).

For $\tau_z = 0$ (assumption 4), eqn $(13)_3$ [with $(8)_1$] is solved for e_z, which is then substituted into $(13)_{1,2}$ to yield

$$\tau_\phi = \frac{E}{1-\nu^2}(e_\phi + \nu e_\theta) - B\alpha p_f,$$
$$\tau_\theta = \frac{E}{1-\nu^2}(e_\theta + \nu e_\phi) - B\alpha p_f. \tag{14}$$

In these equations, Young's modulus E, Poisson's ratio ν, and B are material constants for the drained solid skeleton ($p_f = 0$) (see Table 1). After substitution of eqns (2) and (14) into (9), integration over the shell thickness gives

$$N_\phi = \frac{Eh_s}{1-\nu^2}(\varepsilon_\phi + \nu\varepsilon_\theta) + B\alpha N,$$
$$N_\theta = \frac{Eh_s}{1-\nu^2}(\varepsilon_\theta + \nu\varepsilon_\phi) + B\alpha N,$$
$$M_\phi = Eh_s c^2(\kappa_\phi + \nu\kappa_\theta) + B\alpha M,$$
$$M_\theta = Eh_s c^2(\kappa_\theta + \nu\kappa_\phi) + B\alpha M, \tag{15}$$

where $c = h_s/[12(1-\nu^2)]^{1/2}$ is the reduced shell thickness and

$$N = -\int p_f \, dz, \quad M = -\int p_f z \, dz \tag{16}$$

are the hydrostatic force and moment resultants due to the fluid.

Fluid flow

In three-dimensional consolidation theory, the flow of viscous fluid through a porous elastic solid is governed by Darcy's law (Biot, 1941, 1962)

Table 1. Material coefficients

$\frac{E}{1-\nu^2} = \frac{4\mu(\lambda+\mu)}{\lambda+2\mu}$	$\nu = \frac{\lambda}{2(\lambda+\mu)}$
$B = \frac{2\mu}{\lambda+2\mu} = \frac{1-2\nu}{1-\nu}$	$\beta = \frac{\alpha^2}{\lambda+2\mu} + \frac{1}{F}$
$K = \frac{k}{\mu_f \beta}$	$C = \frac{\alpha B}{\beta}$

$$\frac{k}{\mu_f}\nabla p_f = \phi_f(\dot{\mathbf{u}} - \dot{\mathbf{u}}_f), \tag{17}$$

where k is the intrinsic permeability, μ_f is the fluid viscosity, and dot denotes differentiation with respect to time. Taking the divergence of eqn (17) and using eqns (7) and (8) gives

$$\frac{k}{\mu_f}\nabla^2 p_f = \dot{\zeta}. \tag{18}$$

Next, substituting eqn $(8)_1$ and the expression obtained by solving $(13)_3$ for e_z (with $\tau_z = 0$) into $(13)_4$ gives

$$\zeta = \beta p_f + \alpha B(e_\phi + e_\theta), \tag{19}$$

where β is defined in Table 1. Finally, assumption (5) and eqn (17) imply that the term $p_{f,zz}$ dominates $\nabla^2 p_f$, where comma denotes differentiation with respect to the follower coordinate [see Taber (1992)]. Thus, putting eqns (2) and (19) into (18) yields the fluid flow equation

$$Kp_{f,zz} = \dot{p}_f + \dot{f} + z\dot{g}, \tag{20}$$

where

$$\begin{aligned} f(s,t) &= C(\varepsilon_\phi + \varepsilon_\theta), \\ g(s,t) &= C(\kappa_\phi + \kappa_\theta) \end{aligned} \tag{21}$$

and the effective shell permeability K and the material parameter C are given in Table 1.

As shown in the plate problems considered by Taber (1992), strong transverse gradients in p_f can occur. Thus, eqn (20) is not integrated to produce a resultant form. Solutions to this equation for various surface boundary conditions are given in Appendix A.

CYLINDER WITH OSCILLATING PRESSURE

Analysis

The governing equations for a poroelastic cylinder are derived by setting $\phi = \pi/2$, $r_2 = r$ = constant, and $r_1 \to \infty$. Then, combining eqns (1), (3), (4), (5), (10), (12) and (15) yields

$$Eh_s c^2 h'''' + \frac{Eh_s}{r^2}h = p_{II} - \frac{\nu}{r}V + B\alpha\left(M'' - \frac{1-\nu}{r}N\right). \tag{22}$$

For $\alpha = 0$, this equation reduces to the standard cylindrical shell equation.

To gain insight into some fundamental behavior, we study a cylinder with a harmonically varying internal pressure $p(t)$. The ends of the cylinder are closed ($V = pr/2$ from axial equilibrium), but end effects are ignored. In this case, axial derivatives vanish, and, with transverse inertia included in p_{II}, eqn (22) reduces to

$$\rho\ddot{h} + \frac{Eh_s}{r^2}h = p\left(1 - \frac{\nu}{2}\right) - B\alpha\left(\frac{1-\nu}{r}\right)N, \tag{23}$$

where ρ is the average mass density of the bulk material per unit area of the middle surface.

Table 2. Nondimensional quantities

$\varepsilon = \left(\frac{c}{R}\right)^{1/2}, \quad R = (r_2)_e$	$a = [12(1-\nu^2)]^{1/2}$	$s^* = \frac{s}{R}$
$z^* = \frac{z}{h_s}$	$r^* = \frac{r}{r_e}$	$r_i^* = \frac{r_i}{R}$
$t^* = \frac{tK}{h_s^2}$	$\omega^* = \frac{\omega h_s^2}{K}$	$\rho^* = \frac{\rho K^2 r^4}{E h_s^4 c^2}$
$M_\phi^* = \frac{M_\phi}{E h_s c}$	$H^* = \frac{H \sin\phi_e}{\varepsilon E h_s}$	$V^* = \frac{V}{E h_s}$
$\chi^* = \varepsilon\chi$	$h^* = \frac{h}{r_e}$	$\kappa_i^* = h_s \kappa_i$
$N^* = \frac{N}{\varepsilon E h_s}$	$M^* = \frac{M}{\varepsilon E h_s c}$	$\tau_i^* = \frac{\tau_i}{\varepsilon E a}$
$\lambda^* = \lambda_n h_s$	$f^* = \frac{fR\varepsilon}{E h_s}$	$g^* = \frac{gR\varepsilon}{E}$
$p_i^* = \frac{p_i R\varepsilon}{E h_s}$	$(p^*, p_{n,s}^*, p_{z,\phi}^*, \bar{p}_{1,2}^*) = \frac{r_e}{E h_s}(p, p_{n,s}, p_{z,\phi}, \bar{p}_{1,2})$	
$s_\phi = \frac{\sin\phi}{\sin\phi_e}$	$C^* = \frac{CR\varepsilon}{E h_s}$	

Table 3. Eigenvalues and eigenfunctions

BC	λ_n^*	ϕ_0	ϕ_n
1	$n\pi$	0	$\sin\frac{\lambda_n^*}{2}\cos\lambda_n^* z^* + \cos\frac{\lambda_n^*}{2}\sin\lambda_n^* z^*$
2	$\frac{(2n-1)\pi}{2}$	0	$\sin\frac{\lambda_n^*}{2}\cos\lambda_n^* z^* + \cos\frac{\lambda_n^*}{2}\sin\lambda_n^* z^*$
3	$n\pi$	1	$\cos\frac{\lambda_n^*}{2}\cos\lambda_n^* z^* + \sin\frac{\lambda_n^*}{2}\sin\lambda_n^* z^*$

In terms of the nondimensional quantities defined in Table 2, eqn (23) becomes†

$$\rho^* \ddot{h}^* + h^* = p^*(1-\nu/2) - B\alpha\varepsilon(1-\nu)N^*, \tag{24}$$

where $\varepsilon = (c/r)^{1/2}$ characterizes the shell thickness.

The fluid stress is given by the solution in Appendix A, to which the following refers. For an oscillating internal pressure $\bar{p}_1 = p = p_0 e^{i\omega t}$ ($\bar{p}_2 = 0$), with p_0 a real amplitude and ω the frequency, the steady-state solution is taken in the form

$$(h, N, A_n, a_n, \Psi^{(k)}, f) = (h_0, N_0, A_{n0}, a_{n0}, \Psi_0^{(k)}, f_0)e^{i\omega t}, \tag{25}$$

in which the sub-zero terms are complex. Inserting this equation into (24) and $(A9)_1$ yields

$$h_0(1-\rho\omega^2) = p_0(1-\nu/2) - B\alpha\varepsilon(1-\nu)N_0,$$
$$N_0 = -a(\Sigma A_{n0}\Phi_n^{(0)} + \Psi_0^{(0)}). \tag{26}$$

† Throughout the remainder of this paper [after eqn (24) and including the appendices and figures, but *not the tables*], unless stated otherwise, the nondimensional variables in Table 2 are used *with the asterisks removed*. In some cases, however, the asterisk is kept for emphasis. In addition, prime and dot denote differentiation with respect to s^* and t^*, respectively.

Table 4. Terms of fluid pressure solution

BC	$\Phi_n^{(0)}$	$\Phi_n^{(1)}$	$\Psi^{(0)}$	$\Psi^{(1)}$
1	$(2\lambda_n^*)^{-1}s^2$	$(\lambda_n^*)^{-2}c(2s-\lambda_n^*c)$	$\frac{1}{2}(\bar{p}_1^*+\bar{p}_2^*)$	$\frac{1}{12}(\bar{p}_2^*-\bar{p}_1^*)$
2	$2(\lambda_n^*)^{-1}s^2$	$-(\lambda_n^*)^{-2}s(2s-\lambda_n^*c)$	$\bar{p}_1$	0
3	0	$(\lambda_n^*)^{-2}s(2s-\lambda_n^*c)$	0	0

$s \equiv \sin(\lambda_n^*/2), \quad c \equiv \cos(\lambda_n^*/2)$

where $\Sigma \equiv \sum_{n=0}^{\infty}$ and Table 4 gives $\Phi_n^{(k)}$ and $\Psi_0^{(k)}$. Furthermore, eqns (A5)–(A7) provide the A_{n0}, with f_0 and g_0 given by $(3)_2$, (4), $(15)_1$ with $N_\phi = V$, and (21). For steady state ($t \to \infty$), integration of (A5) then gives

$$A_{n0} = \bar{G}_n a_{n0} \tag{27}$$

with $A_{00} = 0$ and

$$\begin{aligned} \bar{G}_n &= \frac{i\omega}{\lambda_n^2 + i\omega}, \\ a_{n0} &= -2[(\gamma_1 p_0 + f_0)\Phi_n^{(0)} + \delta_1 p_0 \Phi_n^{(1)}], \\ f_0 &= (a^2/24)C(p_0 - 2B\alpha\varepsilon N_0) + C(1-\nu)h_0, \end{aligned} \tag{28}$$

where the λ_n ($= \lambda_n^*$) are given in Table 3, and eqn (A4) provides γ_1 and δ_1. Now, after substituting (27) and (28) into (26), the latter equations can be solved for h_0 and N_0. The result is

$$\begin{aligned} \frac{h_0}{p_0} &= \frac{\gamma(1-\nu/2) + B\alpha\varepsilon(1-\nu)\{\Psi_0^{(0)}/p_0 - \Sigma \bar{G}_n[(2\gamma_1 + Ca^2/12)\Phi_n^{(0)} + 2\delta_1 \Phi_n^{(1)}]\Phi_n^{(0)}\}}{\gamma(1-\rho\omega^2) + 2CB\alpha\varepsilon(1-\nu)^2 \Sigma \bar{G}_n \Phi_n^{(0)2}} \\ \frac{N_0}{p_0} &= [B\alpha\varepsilon(1-\nu)]^{-1}\left[1 - \frac{\nu}{2} - \frac{h_0}{p_0}(1-\rho\omega^2)\right], \end{aligned} \tag{29}$$

where

$$\gamma = a^{-1} + 2CB\alpha\varepsilon(1-\nu^2)\Sigma \bar{G}_n \Phi_n^{(0)2}. \tag{30}$$

Results

For a cylinder with an oscillating internal pressure $p(t)$, three sets of surface boundary conditions (BC) on the fluid are examined [see eqns (A1) and (A4)]. These conditions correspond to specified internal and external pressures on permeable surfaces (# 1), on a permeable inner and impermeable outer surface (# 2), and on two impermeable surfaces (# 3).

In choosing parameter values, we first note that $(\lambda+2\mu)/E = (1-\nu)/[(1+\nu)(1-2\nu)]$, and so the relations in Tables 1 and 2 give

$$C^* = \frac{\alpha}{\varepsilon}\left\{[(1+\nu)[12(1-\nu^2)]^{1/2}]\left(\alpha^2 + \frac{\lambda+2\mu}{F}\right)\right\}^{-1}, \tag{31}$$

which characterizes the fluid–solid coupling [see eqns (20) and (21)]. In addition, Biot and Willis (1957) showed that

$$F = [\phi_f(c_f - c_s) + c_s\alpha]^{-1}, \tag{32}$$

$$\alpha = 1 - c_s/c_{sk}, \tag{33}$$

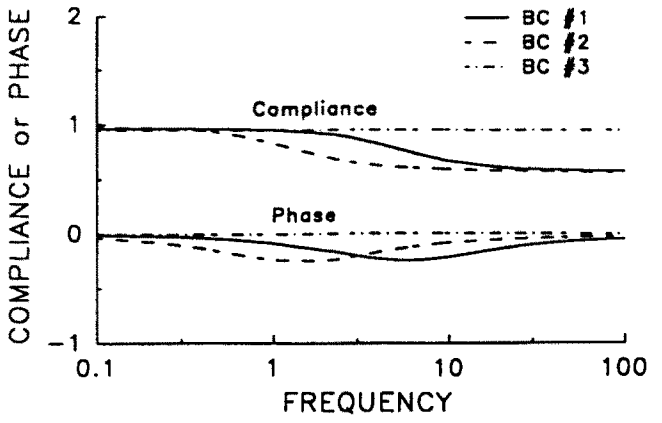

Fig. 2. Magnitude and phase of compliance (h/p) as function of frequency (ω) for poroelastic cylinder with oscillating internal pressure. With end effects and inertia neglected, results are shown for three sets of surface boundary conditions [see eqns (A1) and (A4)].

where c_{sk}, c_s and c_f are the compressibilities of the solid skeleton, the material making up the skeleton, and the fluid, respectively. Here, we consider an incompressible fluid ($c_f = 0$), and so

$$F = [c_s(\alpha - \phi_f)]^{-1}. \tag{34}$$

Equations (31) and (34) show that C^* is maximum when $\alpha = \phi_f$ and, therefore, $F = \infty$. In this case, the fluid effects grow more significant (C^* increases) as the porosity ϕ_f grows smaller (larger flow resistance). Note, however, that eqn (31) now gives

$$C^* \alpha \varepsilon = \{(1+\nu)[12(1-\nu^2)]^{1/2}\}^{-1}, \tag{35}$$

which appears as a grouping in the primary flow resistance terms of eqns (29) and (30). Thus, for a given ν, due to this constraint on the parameters, the shell thickness parameter ε, the relative solid compressibility α, and the fluid–solid coupling coefficient C^* have limited effects on the *dimensionless* membrane-type compliance h_0/p_0. Unless stated otherwise, therefore, the results in this paper are based on the following parameter values for incompressible fluid and solid components ($c_f = c_s = 0$):

$$\varepsilon = 0.01, \quad \nu = 0.1, \quad \alpha = 1, \quad F = \infty, \quad \rho = 0.$$

(Note that, although the solid component is incompressible, $\nu \neq 1/2$ for a porous skeleton.) Also, we found that five terms in the series yield sufficiently accurate results for the range of frequencies studied here.

With inertia neglected, Fig. 2 shows the frequency dependence of the magnitude and phase of the compliance h_0/p_0. For BCs # 1 and # 2, the response resembles that described by Okuno and Kingsbury (1989) for harmonic loading of a poroelastic slab. At low frequencies,† the fluid flows relatively freely through the shell wall and has little effect on the solid displacement, which approaches the elastic value ($h_0/p_0 = 1 - \nu/2 = 0.95$). At high frequencies, the fluid flows little against high resistance, with the fluid pressure building up in the wall (Fig. 3). Through most of the wall, however, the pressure is out of phase with the displacement (and the internal forcing pressure), producing a suction effect as the wall

† The characteristic "consolidation time" is $\tau = h_s^2/K$, and Table 2 gives $\omega^* = \omega\tau$. Thus, "low frequency" (small ω^*) corresponds to a loading time that is large (ω small) compared to the consolidation time.

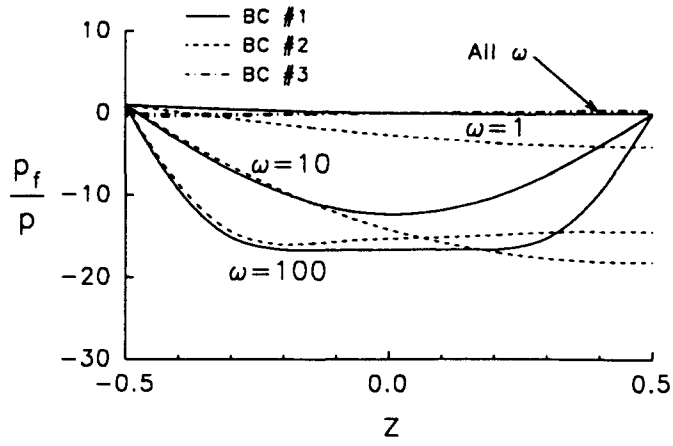

Fig. 3. Fluid pressure distributions in poroelastic cylinder wall.

moves outward. This suction draws the solid skeleton inward, reducing the compliance. The transition between the low- and high-frequency regions, which occurs when the fluid flows against an intermediate resistance, occurs at lower frequencies for BC #2 than for BC #1. For BC #3, fluid cannot leave the wall, and the cylinder behaves essentially like an incompressible shell at all frequencies, with the fluid unable to flow much and having little effect.

The negative fluid pressure at high frequencies (Fig. 3) resembles that found by Jayaraman (1983) for a thick-walled poroelastic cylinder with an oscillating internal pressure.† He described the boundary layers that develop near the shell surfaces as the frequency increases ($\omega = 100$ in Fig. 3). For a step pressure load, Rice and Cleary (1976) discussed a similar phenomenon. When a step load is applied, the solid skeleton instantly deforms elastically, and the pores open before the fluid can flow, producing the suction effect. For small time, the surface boundary conditions on the pressure induce the formation of the boundary layers, where most of the fluid flow occurs due to the steep pressure gradients. Note also that the small fluid pressures for BC #3 contrast with the high pressures found by Taber (1992) for bending of a poroelastic plate with impermeable surfaces. This illustrates the difference between membrane and bending behavior. While little flow occurs during membrane stretching in this case, bending allows fluid to shift from the compressive to the tensile side of the wall.

The total hoop stress (Fig. 4) illustrates the combined effects of the deformation and the fluid pressure. As the frequency increases, the decreasing radial displacement and, therefore, hoop strain produce a lower "contact" stress, which is the stress in eqn $(13)_2$ independent of p_f. While the negative fluid pressure increases the total stress in the shell interior, the peak total stress remains at about the same level as for the case of no fluid.

Finally, Fig. 5 shows the effects of shell inertia for $\rho = 1$. Near the resonant frequency ($\omega = 1$), the fluid resistance damps the deformation, but the magnitude of the damping is not dramatic. At high frequencies, the inertia dominates the response, with the displacement approaching zero.

MATRIX FORMULATION

For general boundary conditions, even for the case of a cylinder, closed-form solutions such as eqn (29) are difficult to find when fluid–solid coupling is important. Thus, taking

† For a thick-walled cylinder, the boundary condition at the inner surface, $\tau_z = -p$, can be significant. This condition is not compatible with the thin-shell approximation $\tau_z = 0$.

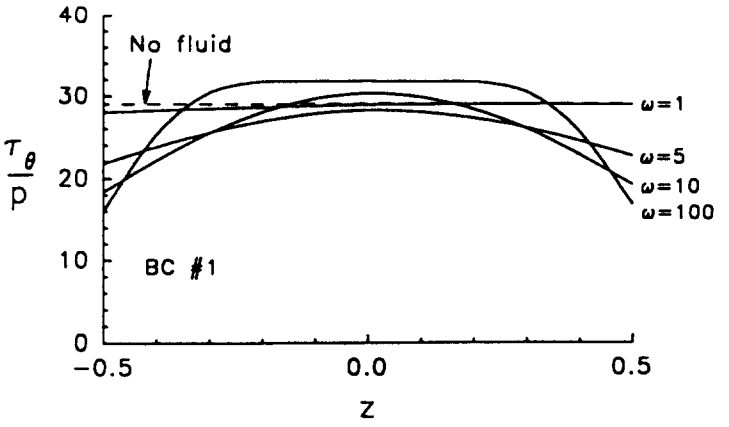

Fig. 4. Total hoop stress distributions in poroelastic cylinder wall.

advantage of previous work in shell theory, we will develop an asymptotic solution for general poroelastic shells of revolution. But first, it is advantageous to express the governing equations in matrix form (Steele and Skogh, 1970). Here, we consider quasi-static motion, i.e. inertia is neglected, and so, given the surface loads, eqn $(12)_1$ can be integrated *a priori* to obtain V. Then, after some manipulation, eqns (3), (4), (5), (10), (12) and (15) can be written in the nondimensional form

$$-\varepsilon \mathbf{y}' + \mathbf{A}\cdot\mathbf{y} = \varepsilon \mathbf{a} + \mathbf{b}, \tag{36}$$

where

$$\mathbf{y} = [M_\phi, H, \chi, h]^{\mathrm{T}} \tag{37}$$

is the solution vector (T denotes transpose) and

$$\begin{aligned} \mathbf{A} &= \mathbf{A}_0 + \varepsilon \mathbf{A}_1 + \varepsilon^2 \mathbf{A}_2, \\ \mathbf{a} &= \mathbf{a}_0 + \varepsilon \mathbf{a}_1, \\ \mathbf{b} &= \varepsilon^{-1}\mathbf{b}_{-1} + \mathbf{b}_0 + \varepsilon \mathbf{b}_1. \end{aligned} \tag{38}$$

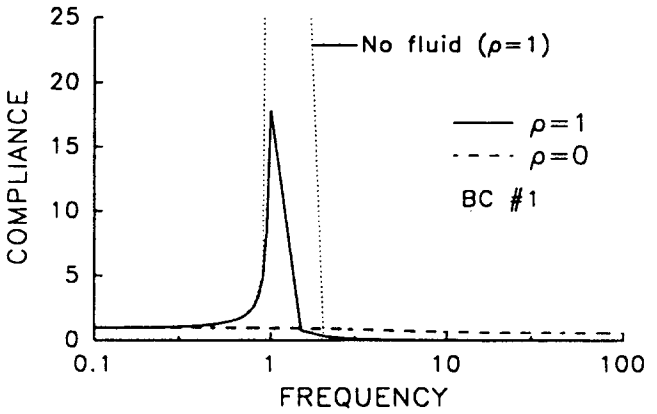

Fig. 5. Effect of inertia on compliance $|h/p|$ of poroelastic cylinder.

In these equations,

$$\mathbf{A}_0 = \begin{bmatrix} 0 & s_\phi & 0 & 0 \\ 0 & 0 & 0 & r^{-2} \\ 1 & 0 & 0 & 0 \\ 0 & 0 & -s_\phi & 0 \end{bmatrix}, \quad \mathbf{A}_1 = -\frac{r'}{r}\begin{bmatrix} 1-\nu & 0 & 0 & 0 \\ 0 & 1-\nu & 0 & 0 \\ 0 & 0 & \nu & 0 \\ 0 & 0 & 0 & \nu \end{bmatrix},$$

$$\mathbf{A}_2 = (1-\nu^2)(r')^2\begin{bmatrix} 0 & 0 & r^{-2} & 0 \\ 0 & 0 & 0 & 0 \\ 0 & 0 & 0 & 0 \\ 0 & 1 & 0 & 0 \end{bmatrix},$$

$$\mathbf{a}_0 = \begin{bmatrix} 0 \\ -(1-\nu)B\alpha N/r \\ B\alpha M \\ 0 \end{bmatrix}, \quad \mathbf{a}_1 = \begin{bmatrix} -(1-\nu)\cos\phi B\alpha M/(r\sin\phi_e) \\ 0 \\ 0 \\ (1-\nu^2)\cos\phi B\alpha N \end{bmatrix},$$

$$\begin{aligned} \mathbf{b}_{-1} &= V\cos\phi[1,0,0,0]^T, \\ \mathbf{b}_0 &= (p_H - \nu V\sin\phi/r)[0,1,0,0]^T, \\ \mathbf{b}_1 &= -(1-\nu^2)Vs_\phi\cos\phi[0,0,0,1]^T, \end{aligned} \tag{39}$$

where

$$s_\phi \equiv \sin\phi/\sin\phi_e \tag{40}$$

and subscript e indicates a reference value at a shell edge. The nondimensional fluid equation (20) is

$$p_{f,zz} = \dot{p}_f + \hat{f} + z\dot{g}, \tag{41}$$

where eqns (21), with $(3)_2$, (4), (10) and $(15)_1$, give

$$\begin{aligned} f(s,t) &= C\left\{\frac{a^2}{12}\left[V\sin\phi + \varepsilon\left(H\frac{\cos\phi}{\sin\phi_e} - B\alpha N\right)\right] + (1-\nu)\frac{h}{r}\right\}, \\ g(s,t) &= Ca\varepsilon\left(\chi' + \frac{\chi\cos\phi}{r\sin\phi_e}\right). \end{aligned} \tag{42}$$

ASYMPTOTIC ANALYSIS

With $\varepsilon = (c/r_2)_e^{1/2}$ being a small parameter for a thin shell, an asymptotic solution can be found in the form of the WKB-type expansions

$$\begin{aligned} \mathbf{y} &= \varepsilon^{-1}\mathbf{y}_{-1} + \mathbf{y}_0 + \varepsilon\mathbf{y}_1 + \cdots + e^{\xi(s)/\varepsilon}(\hat{\mathbf{y}}_0 + \varepsilon\hat{\mathbf{y}}_1 + \cdots), \\ \mathbf{a}_0 &= \boldsymbol{\alpha}_0 + \varepsilon\boldsymbol{\alpha}_1 + \cdots + e^{\xi(s)/\varepsilon}(\hat{\boldsymbol{\alpha}}_0 + \varepsilon\hat{\boldsymbol{\alpha}}_1 + \cdots), \\ \Delta &= \Delta_0 + \varepsilon\Delta_1 + \cdots + e^{\xi(s)/\varepsilon}(\hat{\Delta}_0 + \varepsilon\hat{\Delta}_1 + \cdots), \end{aligned} \tag{43}$$

where $\Delta = (p_f, M, N, f, g)$. In these equations, the terms $\mathbf{y}_i$, $\boldsymbol{\alpha}_i$, Δ_i, etc., are functions of s, and $\xi(s)$ is a decay function. Substituting eqns (38) and (43) into (36) and equating

coefficients of like powers of ε in the usual manner provides the series of interior shell equations

$$\begin{aligned}
&\mathbf{A}_0 \cdot \mathbf{y}_{-1} = \mathbf{b}_{-1},\\
&\mathbf{A}_0 \cdot \mathbf{y}_0 = \mathbf{b}_0 + \mathbf{y}'_{-1} - \mathbf{A}_1 \cdot \mathbf{y}_{-1},\\
&\mathbf{A}_0 \cdot \mathbf{y}_1 = \mathbf{b}_1 + \mathbf{y}'_0 - \mathbf{A}_1 \cdot \mathbf{y}_0 - \mathbf{A}_2 \cdot \mathbf{y}_{-1} + \boldsymbol{\alpha}_0,\\
&\qquad \vdots
\end{aligned} \tag{44}$$

and powers of $\varepsilon e^{\zeta/\varepsilon}$ give the edge-zone equations

$$\begin{aligned}
&(\mathbf{A}_0 - \zeta' \mathbf{I}) \cdot \hat{\mathbf{y}}_0 = 0,\\
&(\mathbf{A}_0 - \zeta' \mathbf{I}) \cdot \hat{\mathbf{y}}_1 = \hat{\mathbf{y}}'_0 - \mathbf{A}_1 \cdot \hat{\mathbf{y}}_0 + \hat{\boldsymbol{\alpha}}_0,\\
&(\mathbf{A}_0 - \zeta' \mathbf{I}) \cdot \hat{\mathbf{y}}_2 = \hat{\mathbf{y}}'_1 - \mathbf{A}_1 \cdot \hat{\mathbf{y}}_1 - \mathbf{A}_2 \cdot \hat{\mathbf{y}}_0 + \hat{\boldsymbol{\alpha}}_1,\\
&\qquad \vdots
\end{aligned} \tag{45}$$

These relations show that the effects of the fluid enter at the level of the first-order terms (second approximation).

Similarly, substitution of eqn $(43)_3$ into (41) provides the fluid equations

$$\begin{aligned}
p_{f_{n+2}} &= \dot{p}_{f_n} + \dot{f}_n + z\dot{g}_n,\\
\hat{p}_{f_{n+2}} &= \dot{\hat{p}}_{f_n} + \dot{\hat{f}}_n + z\dot{\hat{g}}_n,
\end{aligned} \tag{46}$$

for $n = 0, 1, 2, \ldots$, where eqns (42) give, for the first two orders,

$$\begin{aligned}
f_0 &= C\left[\frac{a^2}{12}\left(V \sin\phi + H_{-1}\frac{\cos\phi}{\sin\phi_c}\right) + (1-\nu)\frac{h_0}{r}\right],\\
g_0 &= Ca\chi'_{-1},\\
\hat{f}_0 &= C(1-\nu)\hat{h}_0/r,\\
\hat{g}_0 &= Ca\xi'\hat{\chi}_0,\\
f_1 &= C\left[\frac{a^2}{12}\left(H_0\frac{\cos\phi}{\sin\phi_c} - B\alpha N_0\right) + \frac{1-\nu}{r}h_1\right],\\
g_1 &= Ca\left(\chi'_0 + \frac{\cos\phi}{\sin\phi_c}\frac{\chi_0}{r}\right),\\
\hat{f}_1 &= C\left[\frac{a^2}{12}\left(\hat{H}_0\frac{\cos\phi}{\sin\phi_c} - B\alpha\hat{N}_0\right) + \frac{1-\nu}{r}\hat{h}_1\right],\\
\hat{g}_1 &= Ca\left(\hat{\chi}'_0 + \xi'\hat{\chi}_1 + \frac{\cos\phi}{\sin\phi_c}\frac{\hat{\chi}_0}{r}\right).
\end{aligned} \tag{47}$$

Zero-order shell solution

For the interior solution, the expansion $(43)_1$ suggests that we lump the $O(\varepsilon^{-1})$ and $O(\varepsilon^0)$ terms of $\mathbf{y}$ together for a "zero-order" shell solution. Then, with eqns (39), the first two of (44) give the interior shell terms

$$\mathbf{y}_{-1} = V \sin\phi_e \cot\phi [0, 1, 0, 0]^T,$$

$$\mathbf{y}_0 = r\left[\frac{r_2}{\sin\phi_e} p_z - \left(\frac{r_2}{r_1} + \nu\right)\frac{V}{\sin\phi}\right][0, 0, 0, 1]^T. \tag{48}$$

The corresponding edge-zone solution is given by solving the eigenvalue problem $(45)_1$. The eigenvalues are $\xi'(s) = \Lambda_i$, where

$$\Lambda_1 = \left(\frac{s_\phi}{2r}\right)^{1/2}(1+i), \quad \Lambda_2 = \Lambda_1^c, \quad \Lambda_3 = -\Lambda_1, \quad \Lambda_4 = -\Lambda_1^c, \tag{49}$$

with superscript c denoting the complex conjugate, and the corresponding eigenvectors are

$$\nu_i = [-\Lambda_i^2/s_\phi, 1/(\Lambda_i r^2), -\Lambda_i/s_\phi, 1]^T. \tag{50}$$

For a thin shell ($\varepsilon \ll 1$), the edge zone near a sufficiently steep edge is so narrow that r and ϕ change little within this region (Steele and Skogh, 1970). Thus, we can take $r = s_\phi = 1$ in the edge zone. The Λ_i, therefore, are approximately constant and $\xi(s) \cong \Lambda_i s$. Furthermore, near a shell *lower* edge, the Λ_1 and Λ_2 terms decay toward the shell interior ($s < 0$), and so the solution near this edge can be written [see eqns (43)]†

$$\begin{aligned}
\mathbf{y} &= \varepsilon^{-1}\mathbf{y}_{-1} + \mathbf{y}_0 + \varepsilon\mathbf{y}_1 + \cdots + e^{\Lambda_1 s/\varepsilon}(\hat{\mathbf{y}}_0 + \varepsilon\hat{\mathbf{y}}_1 + \cdots) + e^{\Lambda_2 s/\varepsilon}(\tilde{\mathbf{y}}_0 + \varepsilon\tilde{\mathbf{y}}_1 + \cdots),\\
\mathbf{a}_0 &= \boldsymbol{\alpha}_0 + \varepsilon\boldsymbol{\alpha}_1 + \cdots + e^{\Lambda_1 s/\varepsilon}(\hat{\boldsymbol{\alpha}}_0 + \varepsilon\hat{\boldsymbol{\alpha}}_1 + \cdots) + e^{\Lambda_2 s/\varepsilon}(\tilde{\boldsymbol{\alpha}}_0 + \varepsilon\tilde{\boldsymbol{\alpha}}_1 + \cdots),\\
\Delta &= \Delta_0 + \varepsilon\Delta_1 + \cdots + e^{\Lambda_1 s/\varepsilon}(\hat{\Delta}_0 + \varepsilon\hat{\Delta}_1 + \cdots) + e^{\Lambda_2 s/\varepsilon}(\tilde{\Delta}_0 + \varepsilon\tilde{\Delta}_1 + \cdots).
\end{aligned} \tag{51}$$

Note that we now associate hat terms with Λ_1 and tilde terms with Λ_2.

The zero-order edge-zone terms for the shell can be written as (Steele, 1976a)

$$\hat{\mathbf{y}}_0 = \hat{d}_0(s)\nu_1, \quad \tilde{\mathbf{y}}_0 = \tilde{d}_0(s)\nu_2, \tag{52}$$

where $\hat{d}_0$ and $\tilde{d}_0$ are complex functions of s. These functions are determined by the condition that the right-hand side of eqn $(45)_2$ must be orthogonal to the eigenvectors ρ_i of the transpose of eqn $(45)_1$ (Steele, 1976a, b), i.e.

$$\begin{aligned}
\rho_1 \cdot (\hat{\mathbf{y}}_0' - \mathbf{A}_1 \cdot \hat{\mathbf{y}}_0 + \hat{\boldsymbol{\alpha}}_0) = 0,\\
\rho_2 \cdot (\tilde{\mathbf{y}}_0' - \mathbf{A}_1 \cdot \tilde{\mathbf{y}}_0 + \tilde{\boldsymbol{\alpha}}_0) = 0,
\end{aligned} \tag{53}$$

where

$$(\mathbf{A}_0 - \Lambda_i \mathbf{I})^T \cdot \rho_i = 0 \tag{54}$$

gives

$$\rho_i = [-s_\phi/\Lambda_i^2, \Lambda_i r^2, -s_\phi/\Lambda_i, 1]^T. \tag{55}$$

Inserting eqns (39), (49), (50), (52) and (55) into (53) and noting that $\rho_i \cdot \nu_i = 4$ (all i) yields the differential equations

$$\hat{d}_0' = \hat{B}_1(s)\hat{d}_0 + \hat{B}_2(s), \quad \tilde{d}_0' = \tilde{B}_1(s)\tilde{d}_0 + \tilde{B}_2(s), \tag{56}$$

where

† For an elastic deformation (no fluid flow), $\mathbf{y}$ must be real, and the $\hat{\mathbf{y}}_i$ and $\tilde{\mathbf{y}}_i$ terms can be combined into a single set of edge-zone functions (Steele and Skogh, 1970).

$$\hat{B}_1(s) = \tilde{B}_1(s) = \frac{3r'}{4r} + \frac{s'_\phi}{4s_\phi} - \frac{\cos\phi}{2r\sin\phi_c},$$

$$\hat{B}_2(s) = \frac{1}{4}\left(\frac{s_\phi \hat{\alpha}_{01}}{\Lambda_1^2} - \Lambda_1 r^2 \hat{\alpha}_{02} + \frac{s_\phi}{\Lambda_1}\hat{\alpha}_{03} - \hat{\alpha}_{04}\right),$$

$$\tilde{B}_2(s) = \frac{1}{4}\left(\frac{s_\phi \tilde{\alpha}_{01}}{\Lambda_2^2} - \Lambda_2 r^2 \tilde{\alpha}_{02} + \frac{s_\phi}{\Lambda_2}\tilde{\alpha}_{03} - \tilde{\alpha}_{04}\right). \tag{57}$$

in which the $\hat{\alpha}_{0i}$ and $\tilde{\alpha}_{0i}$ are components of the vectors $\hat{\boldsymbol{\alpha}}_0$ and $\tilde{\boldsymbol{\alpha}}_0$, respectively. Equations (56) are to be solved for $\hat{d}_0(s)$ and $\tilde{d}_0(s)$ subject to the appropriate edge boundary conditions. Within the narrow edge zone, however, $\hat{d}_0$ and $\tilde{d}_0$ change little and can be taken as complex constants. Thus, eqns (56) need not be solved, but they are needed for the $O(\varepsilon)$ terms.

Zero-order fluid solution

With the zero-order shell terms known, the first four of eqns (47) provide f_0, g_0, $\hat{f}_0$, $\hat{g}_0$ (with $\xi' = \Lambda_1$). They also give $\tilde{f}_0$ and $\tilde{g}_0$ if hats are replaced by tildes and $\xi' = \Lambda_2$. Then, eqns (46) for $n = 0$ can be solved for p_{f_0}, $\hat{p}_{f_0}$, and, with hats replaced by tildes, $\tilde{p}_{f_0}$. Since these equations have the same form for each term in the expansion for p_f, the solution in Appendix A is easily adapted, with the appropriate subscripts, hats and tildes placed on all quantities. In addition, care must be taken to apply the appropriate boundary conditions. For p_{f_0}, the conditions of eqn (A1) apply, while $\hat{p}_{f_0} = 0$ and $\tilde{p}_{f_0} = 0$ must replace conditions (I) and (III), i.e. $\bar{p}_1 = \bar{p}_2 = 0$ for these terms. Then, eqn (39) for $\mathbf{a}_0$ gives $\boldsymbol{\alpha}_0$, $\hat{\boldsymbol{\alpha}}_0$ and $\tilde{\boldsymbol{\alpha}}_0$ [see eqn $(51)_2$] with N_0, $\hat{N}_0$, $\tilde{N}_0$, M_0, $\hat{M}_0$ and $\tilde{M}_0$ given by eqns (A9).

First-order shell solution

Next, eqn $(44)_3$ yields the $O(\varepsilon)$ interior shell term

$$\mathbf{y}_1 = [B\alpha M_0, 0, \chi_1, -(1-\nu)B\alpha N_0/r]^{\mathrm{T}}, \tag{58}$$

where

$$\chi_1 = -(\sin\phi)^{-1}[vrp_\phi - V\cot\phi + (rr_2 p_z - Vr_2^2/r_1)'].$$

To find the corresponding edge-zone terms, we express the solution as a linear combination of the eigenfunctions (Steele, 1976a):

$$\hat{\mathbf{y}}_1 = \sum_{i=1}^{4} \hat{d}_i(s)\mathbf{v}_i, \quad \tilde{\mathbf{y}}_1 = \sum_{i=1}^{4} \tilde{d}_i(s)\mathbf{v}_i. \tag{59}$$

Substitution of these expressions into $(45)_2$, dotting both sides with $\boldsymbol{\rho}_j$, and noting that $\boldsymbol{\rho}_j \cdot \mathbf{v}_i = 0$ $(i \neq j)$ and $\mathbf{A}_0 \cdot \mathbf{v}_i = \Lambda_i \mathbf{v}_i$ gives

$$\hat{d}_i = \frac{\boldsymbol{\rho}_i \cdot (\hat{\mathbf{y}}'_0 - \mathbf{A}_1 \cdot \hat{\mathbf{y}}_0 + \hat{\boldsymbol{\alpha}}_0)}{4(\Lambda_i - \Lambda_1)} \quad (i = 2, 3, 4),$$

$$\tilde{d}_i = \frac{\boldsymbol{\rho}_i \cdot (\tilde{\mathbf{y}}'_0 - \mathbf{A}_1 \cdot \tilde{\mathbf{y}}_0 + \tilde{\boldsymbol{\alpha}}_0)}{4(\Lambda_i - \Lambda_2)} \quad (i = 1, 3, 4). \tag{60}$$

The indeterminate functions (in these equations) $\hat{d}_1$ and $\tilde{d}_2$ are taken as complex constants in the boundary layer to be determined by the boundary conditions. With eqns (39), (52), (56), (57) and (60), Appendix B gives the $\hat{d}_i(s)$ and $\tilde{d}_i(s)$ explicitly in terms of known quantities.

First-order fluid solution

Solving eqns (46) for $n = 1$ gives the first-order fluid terms. As in the zero-order fluid solution, the solution in Appendix A can be adapted easily. In this case, $\bar{p}_1 = \bar{p}_2 = 0$ must be used for p_{f_1}, $\hat{p}_{f_1}$ and $\tilde{p}_{f_1}$.

CLAMPED SHELLS WITH OSCILLATING PRESSURE

Analysis

The asymptotic solution now will be specialized to the case of a pressure vessel with ends clamped to rigid circular plates. The internal pressure is $\bar{p}_1 = p_z = p(t) = p_0 e^{i\omega t}$ and $\bar{p}_2 = p_\phi = 0$, and we seek the steady-state response. The boundary conditions at each edge are $h = \chi = 0$, and, at the lower edge, eqns (37) and $(51)_1$ give

$$\begin{aligned} s = 0: \quad & \varepsilon^{-1} h_{-1} + h_0 = \varepsilon^{-1} \chi_{-1} + \chi_0 = 0, \\ & h_n + \hat{h}_n + \tilde{h}_n = \chi_n + \hat{\chi}_n + \tilde{\chi}_n = 0 \quad (n = 1, 2, \ldots), \end{aligned} \tag{61}$$

where, again, the $O(\varepsilon^{-1})$ and $O(\varepsilon^0)$ terms are taken together. Note that a general boundary condition on H could not be satisfied otherwise [see eqns $(43)_1$ and (48)].

First, eqns $(11)_2$ and $(12)_1$ give $V = pr/2$, and eqn (48) provides the "membrane" solution $\mathbf{y}_{-1}$ and $\mathbf{y}_0$. Next, noting that $r = s_\phi = 1$ at a shell edge, we substitute eqns (48)–(50) and (52) into the first line of (61) to find

$$\bar{d}_0 = \bar{d}_0^c = -(h_0)_c(1+i)/2, \tag{62}$$

where $(h_0)_c$ is provided by the edge value of $\mathbf{y}_0$. The resulting zero-order shell solution, which contains no fluid-flow effects, is well known.

With $\mathbf{y}_0$, $\hat{\mathbf{y}}_0$ and $\tilde{\mathbf{y}}_0$ now known, eqns (47) give f_0, g_0, $\hat{f}_0$, etc. Then, eqns (A4) and (A7) yield a_{n0}, $\hat{a}_{n0}$ and $\tilde{a}_{n0}$, which are substituted with (A6) into (A5) to give (for $t \to \infty$)

$$(A_{n0}, \hat{A}_{n0}, \tilde{A}_{n0}) = \bar{G}_n \times (a_{n0}, \hat{a}_{n0}, \tilde{a}_{n0}), \tag{63}$$

where $\bar{G}_n$ is provided by eqn $(28)_1$. The zero-order fluid solution is completed by putting (63) into (A9) to obtain N_0, M_0, $\hat{N}_0$, etc., and eqn $(39)_4$ yields

$$\boldsymbol{\alpha}_0 = \begin{bmatrix} \alpha_{01} \\ \alpha_{02} \\ \alpha_{03} \\ \alpha_{04} \end{bmatrix} = \begin{bmatrix} 0 \\ -(1-\nu) B\alpha N_0/r \\ B\alpha M_0 \\ 0 \end{bmatrix} \tag{64}$$

with similar expressions for $\hat{\boldsymbol{\alpha}}_0$ and $\tilde{\boldsymbol{\alpha}}_0$. In addition, (63), (A1) and (A2) give p_{f_0}, and, with $\psi = 0$, $\hat{p}_{f_0}$ and $\tilde{p}_{f_0}$.

Next, eqn (58) gives $\mathbf{y}_1$, which contains fluid coupling terms. Then, (50), (59) and (B1) give $\hat{\mathbf{y}}_1$ and $\tilde{\mathbf{y}}_1$ with the complex constants $\bar{d}_1$ and $\bar{d}_2$ to be determined with the boundary conditions (61) for $n = 1$. These conditions become

$$\begin{aligned} \sum_{i=1}^{4} (\bar{d}_i + \bar{d}_i) &= -(h_1)_c, \\ \sum_{i=1}^{4} \Lambda_i (\bar{d}_i + \bar{d}_i) &= (\chi_1)_c, \end{aligned} \tag{65}$$

whose solution completes the first-order shell solution.

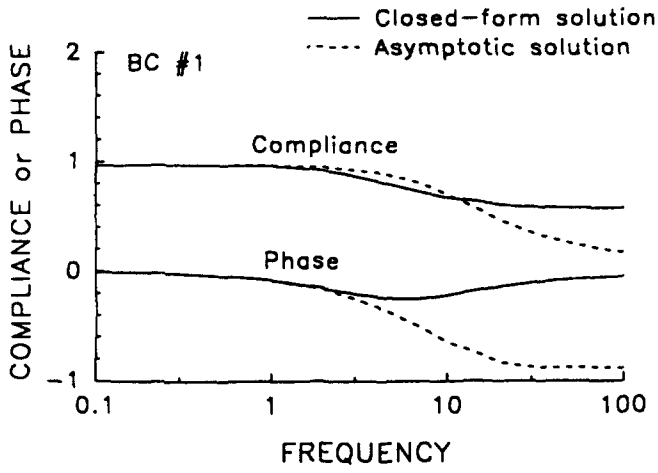

Fig. 6. Comparison of asymptotic and closed form solutions for compliance magnitude and phase far from ends of poroelastic cylinder.

Finally, to obtain the first-order fluid solution, we compute f_1, g_1, $\hat{f}_1$, etc., from eqns (47) and a_{n1}, $\hat{a}_{n1}$ and $\tilde{a}_{n1}$ from (A4) and (A7) with $\bar{p}_1 = \bar{p}_2 = 0$ for all terms. Substitution into (A5) with (A6) yields (for $t \to \infty$)

$$(A_{n1}, \hat{A}_{n1}, \tilde{A}_{n1}) = \bar{G}_n \times (a_{n1}, \hat{a}_{n1}, \tilde{a}_{n1}). \tag{66}$$

Then, eqn (A9) gives N_1, M_1, $\hat{N}_1$, etc., and (66) and (A2) with $\psi = 0$ provide p_{f_1}, $\hat{p}_{f_1}$ and $\tilde{p}_{f_1}$. This completes the solution to $O(\varepsilon)$.

Results

Here, we show results only for the case of a cylinder. As shown in Figs 6 and 7, the validity of the asymptotic solution is limited primarily to frequencies below the transition. In addition, while the (asymptotic) compliance shows the correct qualitative behavior for high frequencies, the phase does not.

As the clamped shell edge is approached from the interior, the resultant force due to the fluid decreases due to the decreasing radial stretch (Fig. 8). At the edge, however, where

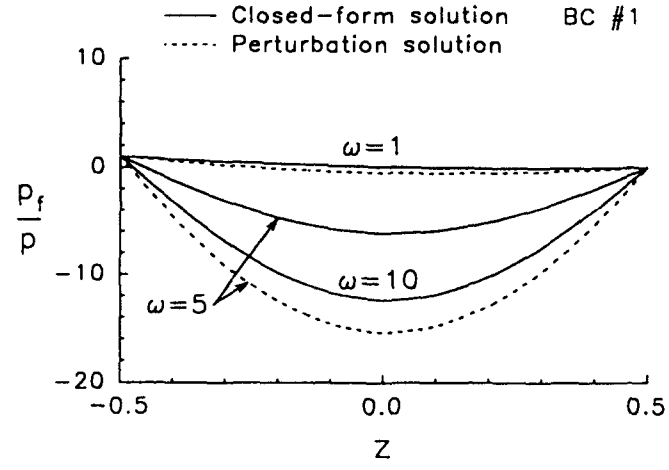

Fig. 7. Comparison of asymptotic and closed form solutions for fluid pressure distributions far from ends of poroelastic cylinder.

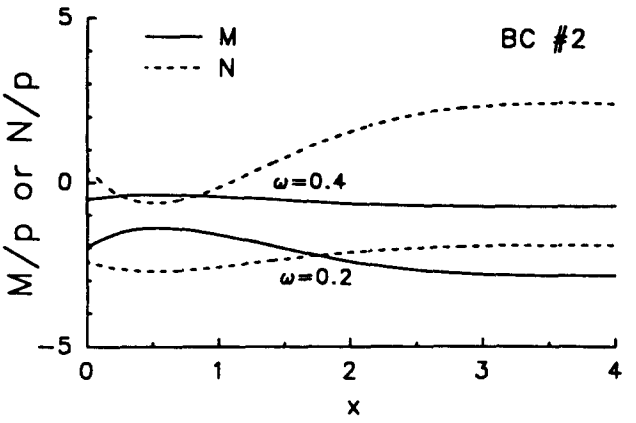

Fig. 8. Axial distributions of fluid stress and moment resultants near clamped end ($x = 0$) of poroelastic cylinder (asymptotic solution). [$x \equiv s^*/(2^{1/2}\varepsilon) = s/(2rc)^{1/2}$.]

bending is strongest, this resultant turns upward again. The effects of bending on M are not as significant. In addition, for the cases studied here, the fluid effects in the edge zone have little effect on the total shell resultants (not shown). Thus, at least in the shell problem studied in this paper, the fluid affects membrane more than bending behavior.

Acknowledgement—This work was supported in part by grant 1 R55 HL46367 from the National Institutes of Health.

REFERENCES

Biot, M. A. (1941). General theory of three-dimensional consolidation. *J. Appl. Phys.* **12**, 155–164.
Biot, M. A. (1962). Mechanics of deformation and acoustic propagation in porous media. *J. Appl. Phys.* **33**, 1482–1498.
Biot, M. A. (1964). Theory of buckling of a porous slab and its thermoelastic analogy. *J. Appl. Mech.* **31**, 194–198.
Biot, M. A. and Willis, D. G. (1957). The elastic coefficients of the theory of consolidation. *J. Appl. Mech.* **24**, 594–601.
Dai, F. and Rajagopal, K. R. (1990). Diffusion of a fluid through an anisotropic thick spherical shell. *Acta Mech.* **85**, 79–97.
Dai, F., Rajagopal, K. R. and Wineman, A. S. (1991). Diffusion through non-linear orthotropic cylinders. *Int. J. Engng Sci.* **29**, 419–445.
Gandhi, M. V., Rajagopal, K. R. and Wineman, A. S. (1987). Some nonlinear diffusion problems within the context of the theory of interacting continua. *Int. J. Engng Sci.* **25**, 1441–1457.
Jayaraman, G. (1983). Water transport in the arterial wall—a theoretical study. *J. Biomech.* **16**, 833–840.
Kenyon, D. E. (1976). The theory for an incompressible solid–fluid mixture. *Arch. Rat. Mech. Anal.* **62**, 131–147.
Okuno, A. and Kingsbury, H. B. (1989). Dynamic modulus of poroelastic materials. *J. Appl. Mech.* **56**, 535–540.
Rajagopal, K. R., Wineman, A. S. and Shi, J. J. (1983). The diffusion of a fluid through a highly elastic spherical membrane. *Int. J. Engng Sci.* **21**, 1171–1183.
Reissner, E. (1950). On axisymmetrical deformations of thin shells of revolution. *Proceedings, Symposia in Applied Mathematics* **3**, *American Mathematical Society* pp. 27–52.
Rice, J. R. and Cleary, M. P. (1976). Stress diffusion solutions for fluid-saturated elastic porous media with compressible constituents. *Rev. Geophys. Space Phys.* **14**, 227–241.
Steele, C. R. (1976a). Theory of shells. ME 241B Course Notes, Stanford University.
Steele, C. R. (1976b). Application of the WKB method in solid mechanics. In *Mechanics Today* (Edited by S. Nemat-Nasser), Vol. 3, pp. 243–295. Pergamon Press, Oxford.
Steele, C. R. and Skogh, J. (1970). Slope discontinuities in pressure vessels. *J. Appl. Mech.* **37**, 587–595.
Taber, L. A. (1992). A theory for transverse deflection of poroelastic plates. *J. Appl. Mech.* (in press).

APPENDIX A

Fluid solution

This appendix presents the solution to the nondimensional fluid flow equation (41) for combinations of the (nondimensional) boundary conditions (BC)

$$z = -\tfrac{1}{2}: \quad p_f = \bar{p}_1(s,t) \quad \text{(I)},$$
$$p_{f,z} = 0 \quad \text{(II)},$$
$$z = \tfrac{1}{2}: \quad p_f = \bar{p}_2(s,t) \quad \text{(III)},$$
$$p_{f,z} = 0 \quad \text{(IV)}, \tag{A1}$$

where $\bar{p}_1$ and $\bar{p}_2$ are prescribed surface pressures for permeable shell surfaces and conditions (II) and (IV) correspond to impermeable surfaces. A series solution to (41) is

$$p_f(s,z,t) = \psi(s,z,t) + \Sigma A_n(s,t)\phi_n(z), \tag{A2}$$

in which

$$\psi(s,z,t) = (\gamma_1 + \delta_1 z)\bar{p}_1(s,t) + (\gamma_2 + \delta_2 z)\bar{p}_2(s,t) \tag{A3}$$

with

$$[\gamma_1, \gamma_2, \delta_1, \delta_2] = \begin{bmatrix} 0.5, & 0.5, & -1, & 1 \\ 1, & 0, & 0, & 0 \\ 0, & 0, & 0, & 0 \end{bmatrix} \quad \begin{matrix} \text{for BC (I)–(III)} & (\#1), \\ \text{for BC (I)–(IV)} & (\#2), \\ \text{for BC (II)–(IV)} & (\#3). \end{matrix} \tag{A4}$$

The eigenfunctions $\phi_n(z)$ and the eigenvalues λ_n are given in Table 3.

The coefficients in eqn (68) are given by

$$A_0(s) = c_0(s),$$
$$A_n(s,t) = c_n(s)G_n(t) + \int_0^t G_n(t-\tau)\dot{a}_n(s,\tau)\,d\tau, \quad n = 1, 2, \ldots, \tag{A5}$$

where dot denotes differentiation with respect to τ and the $c_n(s)$ are to be determined by the initial conditions. (For a steady-state solution, $c_n = 0$). In addition,

$$G_n(t) = e^{-\lambda_n^2 t} \tag{A6}$$

is the relaxation function and

$$a_n(s,t) = -2\int [\psi(s,z,t) + f(s,t) + zg(s,t)]\phi_n(z)\,dz$$
$$= -2[(\gamma_1\bar{p}_1 + \gamma_2\bar{p}_2 + f)\Phi_n^{(0)} + (\delta_1\bar{p}_1 + \delta_2\bar{p}_2 + g)\Phi_n^{(1)}], \tag{A7}$$

where $\int \equiv \int_{-1/2}^{1/2}$, f and g are provided by eqns (21), and

$$\Phi_n^{(k)} \equiv \int \phi_n z^k\,dz \tag{A8}$$

as given in Table 4. Finally, substitution of eqn (A2) into (16) yields

$$N = -a[\Sigma A_n\Phi_n^{(0)} + \Psi^{(0)}]$$
$$M = -a^2[\Sigma A_n\Phi_n^{(1)} + \Psi^{(1)}], \tag{A9}$$

where Table 4 gives

$$\Psi^{(k)} \equiv \int \psi z^k\,dz. \tag{A10}$$

APPENDIX B

First-order shell terms

For a general shell of revolution, the coefficients in eqns (59) are

$$d_1 = \text{complex constant},$$

$$d_2 = \frac{-1+i}{8(2)^{1/2}}d_0(r' + s'_\phi) + \frac{1}{8}\left[\frac{-1-i}{(2)^{1/2}}\dot{x}_{01} + \dot{x}_{02} + i\dot{x}_{03} + \frac{-1+i}{(2)^{1/2}}\dot{x}_{04}\right],$$

$$d_3 = \frac{-1+i}{2(2)^{1/2}}\nu d_0 r' + \frac{1}{8}[(2)^{1/2}\dot{x}_{01} + (1+i)\dot{x}_{02} + (1-i)\dot{x}_{03} + i(2)^{1/2}\dot{x}_{04}],$$

$$d_4 = \frac{-1+i}{2(2)^{1/2}}\nu d_0 r' + \frac{1}{8}[i(2)^{1/2}\dot{x}_{01} + (1-i)\dot{x}_{02} - (1+i)\dot{x}_{03} - (2)^{1/2}\dot{x}_{04}],$$

$$\bar{d}_1 = \frac{-1-i}{2(2)^{1/2}} v\bar{d}_0 r' + \frac{1}{8}[(2)^{1/2}\bar{x}_{01} + (1-i)\bar{x}_{02} + (1+i)\bar{x}_{03} - i(2)^{1/2}\bar{x}_{04}].$$

$\bar{d}_2$ = complex constant.

$$\bar{d}_3 = \frac{-1-i}{2(2)^{1/2}} v\bar{d}_0 r' + \frac{1}{8}[-i(2)^{1/2}\bar{x}_{01} + (1+i)\bar{x}_{02} + (-1+i)\bar{x}_{03} - (2)^{1/2}\bar{x}_{04}].$$

$$\bar{d}_4 = \frac{-1-i}{8(2)^{1/2}}\bar{d}_0(r' + s'_\phi) + \frac{1}{8}\left[\frac{-1+i}{(2)^{1/2}}\bar{x}_{01} + \bar{x}_{02} - i\bar{x}_{03} - \frac{1+i}{(2)^{1/2}}\bar{x}_{04}\right]. \tag{B1}$$